Frequency Selectable Induction Heating Targets

John I. Rodriguez Ruimin He Steven B. Leeb
Laboratory for Electromagnetic and Electronic Systems
Massachusetts Institute of Technology
Cambridge, MA 02139, USA

Abstract— **This paper examines a scheme for developing frequency selectable induction heating targets for stimulating temperature sensitive polymer actuators. "Frequency selectable" implies that each target has a frequency at which it heats preferentially compared to other remaining targets. Single-turn conductors whose critical dimensions are small compared to their associated skin depth (over the frequency range of interest) are examined. One way to achieve selectivity with frequency is by designing each target to have the same self-inductance, while forcing the resistance of each target to differ from the previous one by a specified factor, α. In this way, a target driven at its R/L break-point frequency, will heat by at least a factor of $(\alpha^2+1)/(2\alpha)$ more than the remaining targets.**

I. Background

We are developing an adaptive vibration damper capable of adjusting its natural mechanical frequency to improve damping over a range of vibration frequencies. This damper is an auxiliary spring-mass system and is sometimes called a dynamic vibration absorber (DVA) [1]. When a DVA is mechanically coupled to a vibrating mechanical structure such as an automobile engine, a building, or table, it creates a higher-order mechanical system with at least one resonance and one anti-resonance. At the DVA's natural frequency, the total system experiences an anti-resonance where the mass of the DVA and the mass of the vibrating structure move in counterpoise. The mass of the primary mechanical structure remains relatively stationary while the DVA oscillates as a result of "absorbing" the disturbing vibration.

Typically, a DVA is designed to provide maximum damping at a fixed natural frequency. A more sophisticated DVA can adjust its natural frequency by varying its spring constant with a magnetic actuator, a shape-memory alloy, or some other mechanical scheme [2]. Because the DVA concept applies equally well to both linear and rotational systems, we are exploring an additional approach: a DVA which can adjust its natural frequency by controlling its moment of inertia. Fig. 1(a) shows a simplified model of a rotational DVA with an adjustable moment of inertia. The variable inertia, J_2, can be created using a cylindrical container filled with a variable viscosity fluid. This fluid can be created from a solution of temperature sensitive polymer gel beads suspended in a solvent [3]. Below a certain temperature the gel beads swell, absorbing the surrounding solvent into the polymer

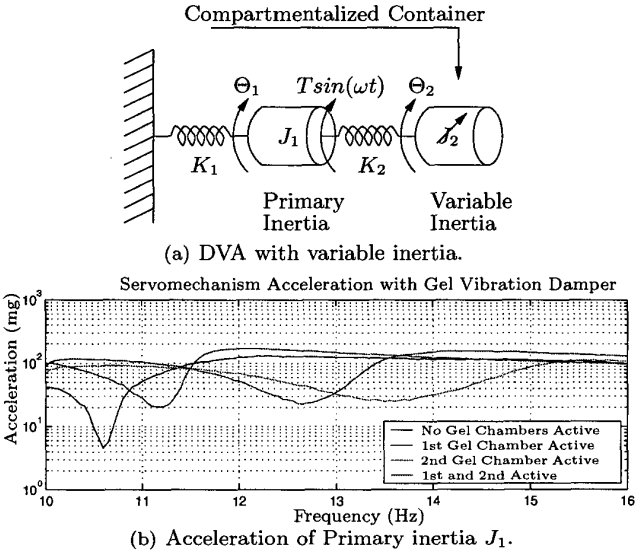

(a) DVA with variable inertia.

(b) Acceleration of Primary inertia J_1.

Fig. 1. Simplified model of gel damper and acceleration response of primary inertia J_1.

matrix (like a sponge). When this happens the gel beads pack tightly in the container, adding significantly to the container's moment of inertia. At higher temperatures the polymer network shrinks, allowing the solvent to flow freely. This effectively decouples the gel-solvent mass and lowers the apparent rotational inertia J_2. By subdividing the container into n multiple compartments of varying gel mass, 2^n anti-resonant states are made possible depending on which compartments are heated. Fig. 1(b) shows peak damping at four different vibration frequencies created by a 2-compartment gel DVA prototype.

II. The Gel Induction Heating System

By design, each gel compartment must be hermetically sealed and allowed to oscillate mechanically with as little external damping as possible. Heating schemes that need to make contact with a gel compartment are therefore undesirable. Induction heating can be used to trigger the gel in each compartment without physical contact [4]. The induction heating system must be capable of selectively heating any combination of gel compartments. One approach to achieve this goal outfits each gel compartment with an induction target that has been designed to heat

0-7803-7754-0/03/$17.00 ©2003 IEEE

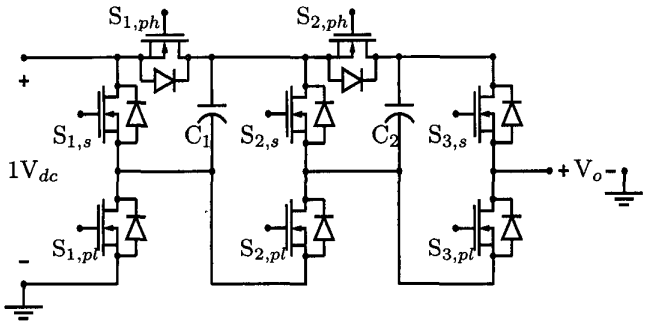

Fig. 2. A four-level Marx inverter.

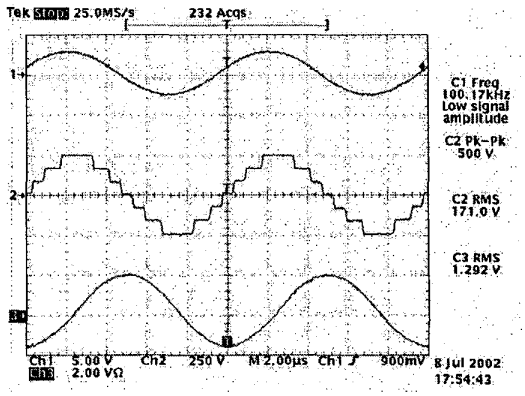

(a) 100KHz Sinewave, inductive load.

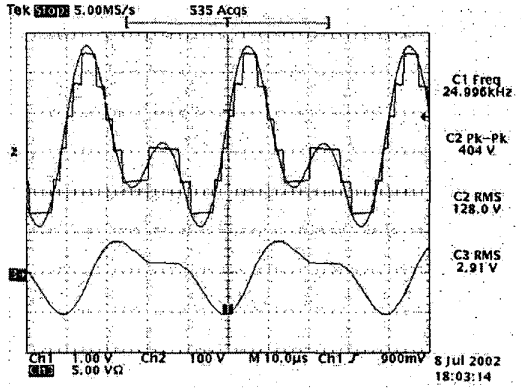

(b) Sum-of-sinewaves (25KHz, 50KHz), inductive load.

Fig. 3. Various Marx inverter waveforms.

preferentially at one frequency (with respect to the other targets). In this case, a single power supply capable of driving a sum-of-sinewaves across a single induction coil could be used to heat the desired combination of inductively coupled targets. This approach does not require a separate induction coil for each target, unlike other multi-load/single-converter induction heating systems [5].

Possible power supplies that could do this include linear power amplifiers or pulse width modulated inverters. A third option, which we are exploring, uses the recently developed Marx inverter topology to approximate the desired sum-of-sinewaves. This multilevel inverter is capable of simultaneously delivering power at multiple frequencies and is the subject of a separate paper [6]. For illustration, one phase leg of a four-level Marx inverter is in Fig. 2. By using two of these phase legs, an induction coil can be driven differentially to generate the necessary waveforms. Some sample waveforms are shown in Fig. 3. Each scope plot shows three waveforms which correspond (from top to bottom) to the desired reference waveform, the multilevel approximation, and the current drawn from the converter when driving an induction heating coil. The reader is referred to [6] for a detailed discussion of this inverter and its operation.

III. Non-Resonant, Frequency Selectable Induction Heating Targets

Frequency selectable induction targets can be subdivided into two categories: resonant and non-resonant. The former involves the creation of a collection of resonant RLC circuits, each inductively coupled to a primary heating coil. In this case, a target's capacitor can be chosen to give that target a unique resonant frequency where it will heat preferentially. In comparison, the non-resonant approach utilizes RL circuits as targets. Varying the target's resistance achieves selective heating, thereby foregoing the need for a resonant capacitor. Although both categories are being explored [7], this paper will focuses on the non-resonant case. "Thin-walled" conductors are prime candidates for use as induction targets in the DVA. The term thin-walled has two meanings. First, it implies that the volume consumed by the target is negligible compared to the gel volume it is heating. Second, it also implies that the conductor thickness is small compared to its skin depth at the frequencies of interest. This leads to a simple circuit model description for each target. The primary coil used to excite these targets can be driven with either a current or voltage source. Both drive conditions are considered.

A. Induction Heating: Current Drive Case

The term "induction heating" usually refers to situations where ohmic dissipation results primarily from current crowding near the conductor's surface as the result of induced eddy currents. In such instances the only way to shield out completely (or terminate) the applied time-varying H-field is to increase the conductor's thickness. Counter-intuitively, a thin-walled conductor whose thickness is small compared to its skin depth, δ, can also act as a good shield. The explanation for this seeming paradox is borrowed from [8] and can be resolved by examining the two cases illustrated in Fig. 4. In each case a perfectly conducting $\supset$ - shaped conductor is driven by a sheet current $K_s = K_o sin(\omega t)$, where it is assumed that each conductor extends a long width w in the direction perpendicular to the page. In case (a) the block of conductor is surrounded

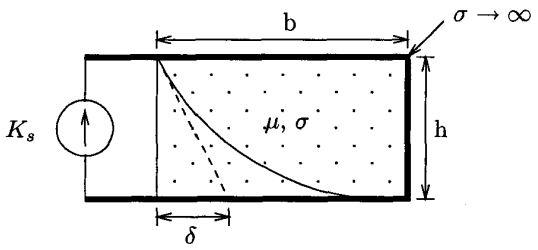

(a) Thick-walled conductor.

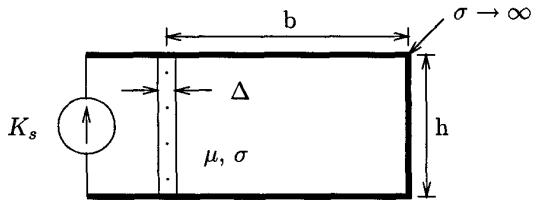

(b) Thin-walled conductor.

Fig. 4. Shielding in thick-walled versus thin-walled conductors.

by the perfectly conducting $\supset$ - shaped conductor. At low frequencies the currents flow around the perfect conductor; as the frequency is increased, however, currents begin to flow along the left edge of the block where the reactance is lower. If we assume that the $\delta << b$ such that the current magnitude decays exponentially as shown, then the interior of the block is effectively shielded from the H-field at points where the current has decayed to zero. In case (b) where the conductor thickness $\Delta << \delta$, the conductor forms a current divider with the $\supset$ - shaped conductor. If we define the conductance per unit width, $G = \sigma\Delta/h$, and the inductance times a unit width, $L = \mu bh$, for these structures, the current through the thin wall is

$$K_{thin-wall} = \frac{j\omega LG}{1 + j\omega LG} K_o. \tag{1}$$

Note that this transfer function is identical in form to the output current flowing through the resistive leg of a parallel RL circuit that is driven by a current source. Similarly, a thin-walled conductor can be modeled as a parallel RL circuit provided that $\Delta << \delta$.

If each target is designed to have a similar self-inductance, L_n, but a different resistance, R_n, a frequency selectable heating scheme can be devised. An example is shown in Fig. 5. Three shorted wires or sheets of different alloys form single-turn inductors with different resistances. All three are coupled to a single primary induction coil, with inductance, L_1, and resistance, R_1. If the primary coil is driven by a sinusoidal current with amplitude I_1 and the cross-coupling between induction targets is negligible, the power delivered to a target is independent of the power delivered to any remaining target. In this case we may

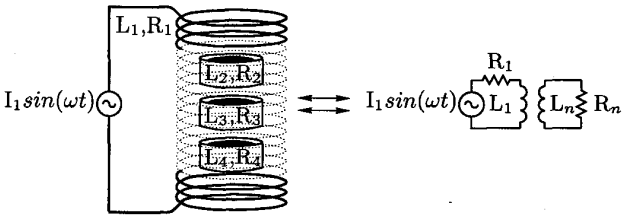

Fig. 5. Induction heating circuit for 3 different targets.

express the time average power dissipated in a target n as

$$< P_n(\omega) >= \frac{(I_1 K_n \omega)^2 L_1 L_n R_n}{2[(L_n\omega)^2 + R_n^2]}. \tag{2}$$

The term K_n represents the coupling coefficient between the primary coil and target n, and is defined using the mutual inductance, L_{1n}, between L_1 and L_n:

$$K_n = \frac{L_{1n}}{\sqrt{L_1 L_n}}. \tag{3}$$

If target n (2, 3, or 4) is driven at its -3dB break-point frequency in Hertz

$$f_n = \frac{\omega_n}{2\pi} = \frac{R_n}{2\pi L_n}, \tag{4}$$

the equation for time average power reduces to the following:

$$< P_n(f_n) >= \frac{\pi}{2} L_1 (K_n \cdot I_1)^2 f_n, \tag{5}$$

It is interesting to note from this equation that once the break-point frequency of the target is established the only way to increase power dissipation is by increasing the primary side current or inductance, or improving the coupling between the coil and target. The absolute values of the target's self-inductance or resistance are irrelevant as only their ratio matters. If the targets are further constrained so that the resistance between one target and the next differs by a factor of α, i.e. $R_{n+1} = \alpha R_n$, it can be shown that the time-averaged power dissipated in R_n when driven at its break-point frequency with respect to the closest higher frequency target is

$$< P_n(\omega_n) >= \frac{\alpha^2 + 1}{2\alpha} \left(\frac{K_n}{K_{n+1}}\right)^2 < P_{n+1}(\omega_n) > . \tag{6}$$

Similarly, the time-averaged power dissipated in R_n with respect to the closest lower frequency target is

$$< P_n(\omega_n) >= \frac{\alpha^2 + 1}{2\alpha} \left(\frac{K_n}{K_{n-1}}\right)^2 < P_{n-1}(\omega_n) > . \tag{7}$$

These results are more readily appreciated by plotting the power profiles for three hypothetical targets versus frequency as shown in Fig. 6(a). The coupling coefficient of all targets has been chosen equal to 0.3 and the three targets have break-point frequencies that are separated by factors of 5, specifically 4KHz, 20KHz, and 100KHz. Under these constraints each target experiences preferential heating

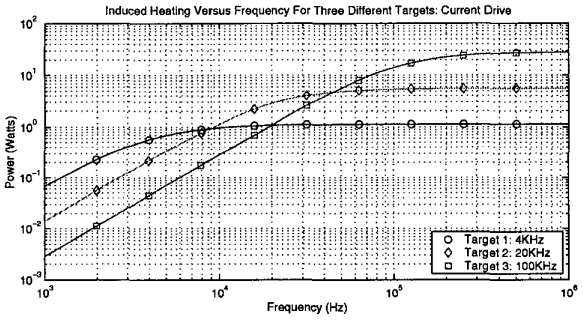

(a) Power profiles for 3 different targets.

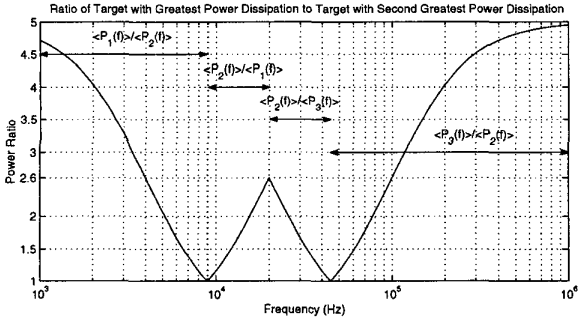

(b) Ratio of delivered power between targets.

Fig. 6. Induction heating power curves versus frequency for 3 different targets assuming a current source drive of $I_1 = 1A$.

with respect to the remaining targets over some frequency range. The extent of preferential heating is given as a ratio in Fig. 6(b) for this example. Because of the identical coupling and the even spacing in break-point frequencies, each target experiences power dissipation of at least 2.6 times more than any of the remaining targets when driven at its break-point frequency– as suggested by equations (6) and (7). Equation (5) makes apparent that a fixed current results in higher power dissipation at higher frequencies. In order to equalize the absolute power delivered to all targets the amplitude of the current driving the primary coil must be controlled via the following relationship:

$$I_1(\omega_{n+1}) = \frac{1}{\sqrt{\alpha}} \frac{K_n}{K_{n+1}} I_1(\omega_n). \quad (8)$$

B. Experimental Setup: Thin-walled Cylindrical Shells

To test these models, three thin-walled shells each measuring 1.25" in diameter and 1.00" in length were constructed by soldering or brazing together a single piece of 110 annealed copper, alloy 260 brass, or 302 stainless steel shim respectively. These dimensions lead to a self-inductance of about 25nH for each target. In order to achieve a desired separation in resistance of $\alpha \approx 5$, these conductors were chosen with the following respective thicknesses (Δ): 3mils, 2mils, and 4mils. These values result in nominal break-point frequencies of 5.6KHz, 30.2KHz, and 169.2KHz, respectively. The power dissipation as a function of frequency for each target was

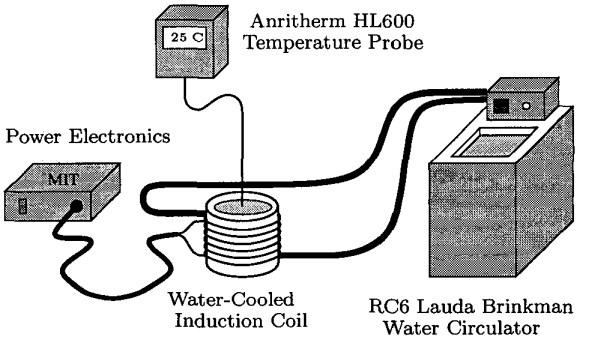

(a) Calorimetry test setup.

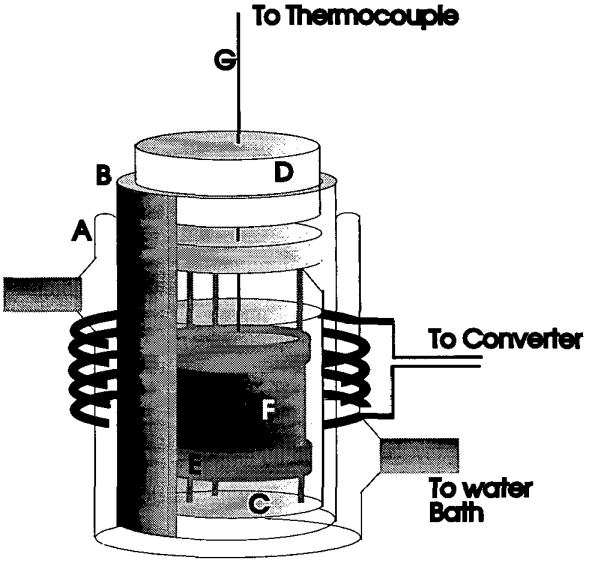

(b) Closeup of test vessel.

Fig. 7. Calorimetry test setup with closeup of the test vessel.

determined via a careful calorimetry experiment and then tabulated.

Fig. 7(a) shows the overall setup for the calorimetry experiment while Fig. 7(b) shows a closeup of the test vessel. The test is carried out using an induction coil which has been wrapped around a water-cooled glass former (A) that is maintained at a constant 25.0°C by a Lauda Brinkman water circulator. This is done to insure that none of the power dissipated in the induction coil influences the heating of the induction target (F). The induction target is designed to fit onto an acrylic former (E) which in turn sits in a water-filled test jar (C). This arrangement insures that the position of the target with respect to the primary coil is fixed, thereby maintaining a constant coupling coefficient from target to target. A thermocouple probe (G) fits through a small hole in the top of the test jar and is used to measure the temperature of the heated water. To minimize heat transfer between the test jar and the external surroundings, a thick layer of insulating material (B) separates the side walls and

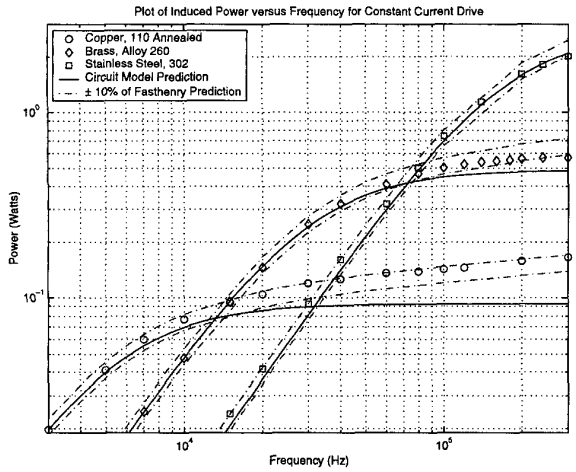

Fig. 8. Calorimetry results for 3 different induction heating targets.

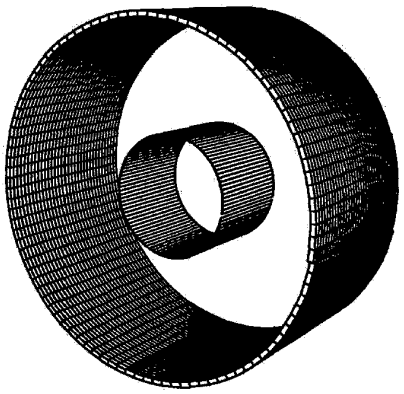

Fig. 9. 3-D Model of the primary induction coil and an induction target as used in the calorimetry experiment.

bottom of the test jar from the water-cooled glass former while a styrofoam cap (D) covers the top of the jar.

The induction coil is driven by a multilevel sine-wave approximation similar to the one shown in Fig. 3(a) and the frequency of the sine-wave is varied from 3KHz to 300KHz. In order to keep the amplitude of the primary current constant, the voltage amplitude is manually servoed at each frequency. At the desired frequency a fixed quantity of water (165.2 grams) is heated for exactly one hour starting from the moment it reaches 25.0°C. At the end of this period the container is shaken to equalize the internal temperature and the final temperature is measured by the digital thermometer and recorded. Although in principle the power delivered could be estimated based on the change in temperature by using the mass and specific heat of the water, acrylic former, and glass walls this method would only be accurate if no energy is lost to the external environment. A better way of calibrating the power delivered from the change in temperature is to run the experiment using a well defined source of power for exactly one hour. This was done by dissipating a fixed amount of power in a resistor immersed in the water during separate tests.

C. Results: Thin-walled Cylindrical Shells

Fig. 8 shows the results of the calorimetry experiment for the three test metals. The simple RL model accurately predicts the power dissipation of the stainless steel and brass conductors over a wide range of frequencies. In the case of the copper target, there is a noticeable discrepancy, especially at high frequencies. This discrepancy is attributable to the fact that the skin depth is approaching the conductor thickness (at $f = 300KHz$, $\delta_{cu} \approx 1.6\Delta_{cu}$). As an additional check, a 3-D model of the induction coil and target shown in Fig. 9 was evaluated using the 3-D field solver, Fasthenry [9] in order to model skin effect on the AC impedance of each target. The dashed lines in Fig. 8 represent a variation in the Fasthenry prediction of $\pm 10\%$, and as shown, almost completely bound all of the calorimetry data. Variation in the calorimetry data can be attributed to $\pm 10\%$ manufacturing tolerances in the shim thickness as well as measurement error and unmodelled parasitics, such as contact resistance from soldering or brazing each conductor into a cylindrical shell.

D. Induction Heating: Voltage Drive Case

The current driven case resulted in easy to understand relationships governing the power dissipation in each target. However, the Marx inverter naturally applies a voltage not a current source drive. The analysis of a voltage driven system is slightly more complicated since the primary current is now a function of the aggregate impedance the converter must drive. This means that, unlike the current mode case, the absolute power delivered to a target can not be analyzed without taking into consideration the effect of all the targets, even if the cross-coupling between targets is negligible. Fortunately, the ratio of power delivered between loads as indicated in Fig. 6 remains unchanged whether a voltage or current drive is employed.

Because of the multiple output nature of this system the voltage mode case can be conveniently described using the following state-space description,

$$\begin{bmatrix} \dot{I} \end{bmatrix} = \begin{bmatrix} -L^{-1}R \end{bmatrix} \begin{bmatrix} I \end{bmatrix} + \begin{bmatrix} L^{-1} \end{bmatrix} \begin{bmatrix} V_{in} \\ 0 \end{bmatrix}, \quad (9)$$

where V_{in} is the amplitude of the input voltage and L is the general inductance matrix of the system, which for the three target case takes the following form:

$$L = \begin{vmatrix} L_{11} & L_{12} & L_{13} & L_{14} \\ L_{21} & L_{22} & L_{23} & L_{24} \\ L_{31} & L_{32} & L_{33} & L_{34} \\ L_{41} & L_{42} & L_{43} & L_{44} \end{vmatrix}. \quad (10)$$

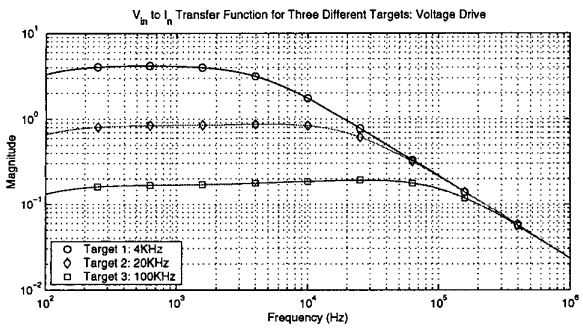

(a) Transfer function for 3 different targets.

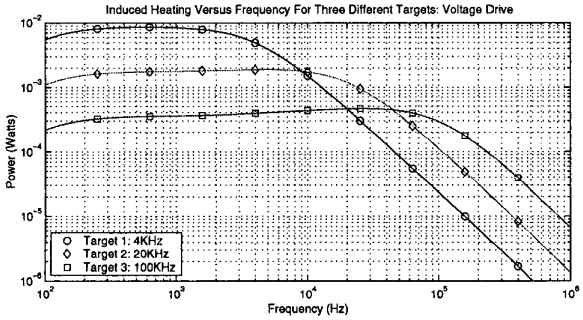

(b) Power profiles for 3 different targets.

Fig. 10. V_{in}-to-I_n transfer function and power curves versus frequency for 3 different targets assuming a voltage drive, V_{in}=1V.

Likewise, the resistance matrix R for the primary coil and the three induction targets (n=2, 3, and 4) is

$$R = \begin{vmatrix} R_1 & 0 & 0 & 0 \\ 0 & R_2 & 0 & 0 \\ 0 & 0 & R_3 & 0 \\ 0 & 0 & 0 & R_4 \end{vmatrix}. \quad (11)$$

Using (9) the transfer function from V_{in}-to-I_n, were I_n denotes the current in conductor n, for the hypothetical system described in Fig. 6, was calculated in Matlab and is shown in Fig. 10(a). Because the induction coil's impedance grows with frequency (ignoring the effect of parasitic capacitance) the current in each load must drop off at high frequencies. This results in the dissipated power curves for each load shown in Fig. 10(b) where, unlike the current mode case, power decreases with increasing frequency. Note that power also rolls off at low frequencies because of the finite resistance from the primary coil. In the low frequency limit the current through the induction coil approaches a constant value, hence for low frequencies the system behavior resembles that of the current mode case. If the effective resistance of a target is known and does not vary significantly with frequency, the induction heating profile for that target can be inferred from its V_{in}-to-I_n transfer function. For a sinusoidal voltage drive of amplitude V_{in} the current, I_n, flowing in conductor n can be determined and used to calculate the power dissipated

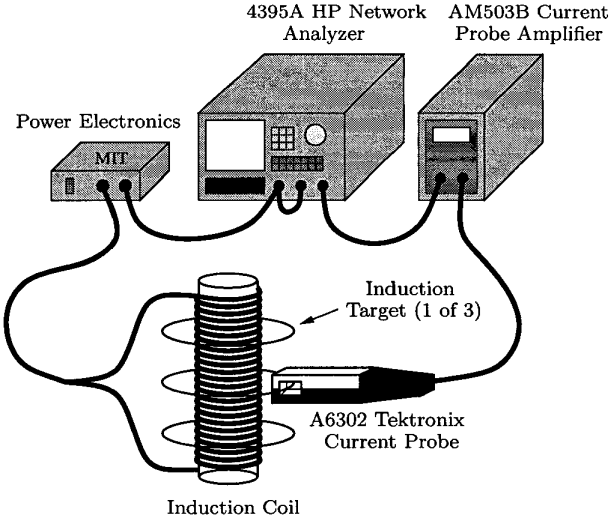

Fig. 11. Multi-wire induction heating experiment.

according to the relationship,

$$< P_n(\omega) >= \frac{1}{2} I_n(\omega)^2 R_n. \quad (12)$$

E. Experimental Setup: Thin Wire Loops

As a final experiment, a multi-target system was built using 3 different metal wires: copper, alloy 90 and alloy 800[1]. For this experiment each wire had a diameter of 0.08118 cm (20AWG) and was formed into a loop measuring 6.00cm in diameter. Each resulting target had a self-inductance of $0.167\mu H$. The resistances of these alloys are roughly factors of 8-9 apart and were chosen to yield nominal break-point frequencies of 5.98KHz, 51.9KHz, and 461.6KHz respectively. The purpose of this experiment was not to measure power directly but to characterize the V_{in}-to-I_n transfer function for all of the targets so that power could be inferred later. Fig. 11 illustrates the entire system. In this setup, all three wire loops are arranged on a PVC former (not shown) and coupled to a $205\mu H$ induction coil. The center's of the targets and the induction coil are offset in order to accommodate a A6302 Tektronix current probe. An HP 4395A network analyzer determines the transfer function by sweeping the voltage reference that generates the multilevel sine-wave approximation impressed across the induction coil. The current in each target is then measured via the current probe and amplified before being passed back to the network analyzer.

In order to calculate the theoretical transfer functions for this system, a 3-D model of this system was generated and passed to Fasthenry to estimate the inductance matrix for the system. A view of the model used is shown in Fig. 12. In principle the mutual inductances could have been estimated in a variety of ways, including direct evaluation

[1]Alloy 90 and alloy 800 are commercially available resistance wires.

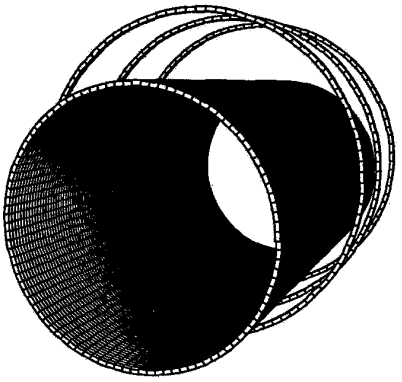

Fig. 12. 3-D Model of the primary induction coil and targets as used in the multi-wire induction heating experiment.

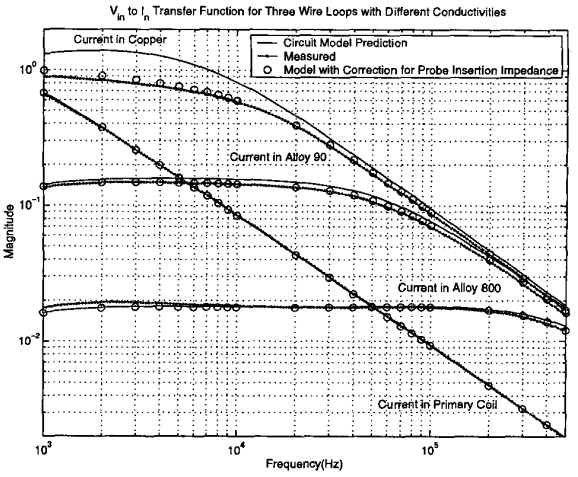

Fig. 13. Results of multi-wire induction heating experiment.

of the Neumann formula or with a numerical approach such as a mesh-matrix technique [10].

F. Results: Thin Wire Loops

The experimental magnitude response of the system is shown in Fig. 13. A discrepancy between the circuit model and the measured data was apparent for the lower resistance wires, especially the copper wire. This discrepancy is the result of the additional insertion loss added to the wire target by the current probe during the measurement. Because the resistance of the copper wire ($R_{cu} = 6.28m\Omega$) is comparable to the insertion loss associated with the current probe it cannot be ignored. This effect is less noticeable for the remaining alloys because of their lower conductivities. To account for this measurement error, the insertion impedance of the probe was characterized over the frequency range in question and then used to calculate what the new magnitude response would be. After allowing for this correction the measurements agree within about $\pm 10\%$ over the majority of frequency range. For about $5KHz$ and higher the agreement is closer to $\pm 5\%$. The increased error at low frequencies is due to unmodelled dynamics from the multilevel inverter as the output capacitors of this stage begin to have some effect.

IV. Conclusion

Frequency selectable induction heating targets can be constructed using single-turn conductors whose critical dimensions are small compared to the skin depth at the frequency range of interest. If these single-turn conductors have similar self-inductances, with R/L break-point frequencies that are spaced evenly by factors of α, frequency selectivity can be achieved. That is a target driven at its break-point frequency will heat by an amount of $(\alpha^2 + 1)/(2\alpha)$ more than the remaining targets. These results were experimentally demonstrated for two types of induction targets, thin-walled cylindrical shells and thin wire loops.

One application of these targets is a tunable vibration damper we are developing. The damper relies on the fact that a rotating container filled with a variable viscosity material can alter its moment of inertia. In this case the rotating container consists of a set of individual compartments filled with a thermally responsive gel. Thermal stimulation of the different compartments allows the damper to adjust the location of its anti-resonant frequency. One way to thermally activate these compartments is by outfitting each chamber with a frequency selectable induction target. Any combination of chambers can then be simultaneously heated by the primary induction coil if it is driven at the appropriate frequencies with a voltage sum-of-sinewaves .

This multi-frequency, multi-target approach can be used in a wide range of applications, including medical and industrial processes, to provide a wide range of spatial temperature control. One such application is the treatment of deep-seated tumors using hyperthermia [11]-[14]. Currently, the generation of a desired spatial temperature gradient requires a complicated distribution of identical induction targets. The availability of frequency selectable targets would allow greater flexibility in the distribution of targets, especially, because the temperature profile can now be modified post target distribution simply by controlling the drive voltage across the primary induction coil.

Acknowledgements

The authors gratefully acknowledge the support of the National Science Foundation through a MRSEC grant to MIT's Center for Materials Science and Engineering, a grant from the Grainger Foundation, and support from the Ford Motor Company.

REFERENCES

[1] Harris C., Crede C.,"Shock and Vibration Handbook (vol.1), McGrawHill, New York, 1961.

[2] Christopher Ting-Kong, "Design of an Adaptive Dynamic Vibration Absorber," *M.eng. Thesis,* Department of Mechanical Engineering, The University of Adelaide, South Australia 5005, April 1999.

[3] T. Tanaka, "Gels," Scientific American, vol. 244, no. 1, pp. 124-138, Jan. 1981

[4] Jackson, D.K.; Leeb, S.B.; Mitwalli, A.H.; Narvaez, P.; Fusco, D.; Lupton, E.C., Jr.; "Power electronic drives for magnetically triggered gels," ndustrial Electronics, IEEE Transactions on , Volume: 44 Issue: 2 , Apr 1997 Page(s): 217 -225

[5] F. Forest, E. Laboure, F. Costa, J.Y. Gaspard, "Principle of a multi-load/single converter system for low power induction heating," IEEE Trans. Power Electronics, vol.15, no. 2, pp. 223-230, March 2000.

[6] J.I. Rodriguez and S.B. Leeb, "A Multilevel Inverter Topology for Inductive Power Transfer," Applied Power Electronics Conference, 2003. APEC '03. Eighteenth Annual, pp 1118-1126.

[7] J. I. Rodriguez, "A Multi-Frequency Induction Heating System for a Thermally Triggered Gel Polymer Dynamic Vibration Absorber," *Ph.D. Thesis,* Massachusetts Institute of Technology, Expected June, 2003.

[8] H. A. Haus, and J. R. Melcher, *Electromagnetic Fields and Energy,* Prentice-Hall, 1989 ,pp. 446-447.

[9] Kamon, M.; Ttsuk, M.J.; White, J.K. "FASTHENRY:a multipole-accelerated 3-D inductance extraction program," Microwave Theory and Techniques, IEEE Transactions on , Volume: 42 Issue: 9 Part: 1-2 , Sept. 1994 Page(s): 1750 -1758

[10] Ki-Bong Kim; Levi, E.; Zabar, Z.; Birenbaum, L.; "Mutual inductance of noncoaxial circular coils with constant current density," Magnetics, IEEE Transactions on , Volume: 33 Issue: 5 , Sep 1997 Page(s): 4303 -4309

[11] P.I.Stauffer, T.C. Cetas, A.M. Fletcher, D.W. DeYoung, M.W. Dewhirst, J.R. Oleson, R.B. Roemer, "Observations on the user of Ferromagnetic Implants for inducing Hyperthermia," Biomedical Engineering, IEEE Transactions on, Volume: BME31, no. 1, Feb 1984, pp.76-90

[12] P.I.Stauffer, T.C. Cetas, R.C. Jones, "Magnetic Induction Heating of Ferromagnetic Implants for Inducing Localized Hyperthermia in Deep-Seated Tumors," Biomedical Engineering, IEEE Transactions on, Volume: BME31, no. 2, Feb 1984, pp.235-251

[13] A.Y. Matloubieh, R.B. Roemer, T.C. Cetas, "Numerical Simulation of Magnetic Induction Heating of Tumors with Ferromagnetic Seed Implants," Biomedical Engineering, IEEE Transactions on, Volume: BME31, no. 2, Feb 1984, pp.227-234

[14] Kimura, I.; Katsuki, T.; "VLF induction heating for clinical hyperthermia,"' Magnetics, IEEE Transactions on , Volume: 22 Issue: 6 , Nov 1986 Page(s): 1897 -1900

[15] F. Forest, E. Laboure, F. Costa, J.Y. Gaspard, "Principle Breed of Power Converters," IEEE Trans. Ind. Applicat., vol. 32, no. 3, pp. 509-517, May/June 1996.

[16] F.Z. Peng, "A Generalized Multilevel Inverter Topology with Self Voltage Balancing," IEEE Trans. Ind. Applicat., vol. 37, no. 2, pp. 611-618, March/April 2001.

[17] A. Nabae, I. Takahashi, and H. Akagi, "A New Neutral-Point-Clamped Inverter", IEEE Trans. Ind. Applicat., vol. IA-17, no. 5, pp. 518-523, September/October 1981.

[18] D. Jackson, "Inductively Coupled Power Transfer for Electromechanical Systems," *Ph.D. Thesis,* Massachusetts Institute of Technology, May, 1998.

[19] J.G. Kassakian, M.F. Schlecht, and G.C. Verghese, *Principles of Power Electronics,* Addison-Wesley, 1991.